ELSEVIER

Spectrochimica Acta Part A 53 (1997) 1705–1712

SPECTROCHIMICA ACTA PART A

High resolution photoacoustic spectrum of AsH_3 ($600A_1/E$) bands

Jia-xiang Han [a], Oleg N. Ulenikov [b], Sergi Yurchinko [b], Lu-yuan Hao [a], Xiao-gang Wang [a], Qing-shi Zhu [a,*]

[a] *Department of Chemical Physics, University of Science and Technology of China, Hefei 230026, People's Republic of China*
[b] *Laboratory of Molecular Spectroscopy, Physics Department, Tomsk State University, Tomsk 634050, Russia*

Received 18 September 1996; received in revised form 15 February 1997; accepted 15 February 1997

Abstract

The high resolution spectrum of arsine in the region of 11 470–11 650 cm^{-1} was recorded by a sensitive laser photoacoustic apparatus. The vibration–rotation transitions of the local mode pair of bands ($600A_1/E$) were assigned and their major vibration–rotation parameters were obtained by least-square fitting. The results indicate that the selection rules on the quantum number k have no effect in the high J values owing to strong Coriolis coupling. In addition, the intensities of vib–rotational transitions were estimated by comparison with standard water lines. © 1997 Elsevier Science B.V.

Keywords: Photoacoustic spectroscopy; Arsine; Vibration–rotational transitions

1. Introduction

It is difficult to record the high resolution spectrum of high overtones in practice owing to the small transition dipole moment from ground state to overtones and the need to record at low sample pressure to avoid pressure broadening. Recently, intensive experimental work has been carried out on the high resolution spectra of stretching overtones, taking advantage of interferometric and various highly sensitive intracavity laser spectroscopic techniques.

The high resolution Fourier transform spectrometer combining with White-type multipath absorption cell has proved to be a very effective tool for the high resolution spectroscopic study of the first few overtones, up to $v = 4$ or 5 (about 12 000 cm^{-1}). Taking advantage of this technique, Zhu and co-workers have recorded the high resolution spectra of GeH_4 $v = 3$ [1,2] and SiH_4 $v = 3$–5 [3,4] stretching overtones. It has also been used to study the stretching overtones of SnH_4 [5–8], SbH_3 [9–11], AsH_3 [12–14] and H_2Se [15,16], etc.

Intracavity laser absorption spectroscopy (ICLAS) is a particularly good technique for high overtone spectroscopy in the visible region [17].

* Corresponding author.

PII S1386-1425(97)00067-X

This technique is highly sensitive and quantitative since it is based on the high sensitivity of a broadband laser to intracavity frequency selective losses due to the absorber contained in an intracavity cell. The high resolution spectrum of GeH_4 and SiH_4 $v=6-7$ overtone bands was obtained by the ICLAS technique [18,19] with an effective pathlength of $l_{eff}=5.25$ km and the dyes styryl 9 and pyridine 2, respectively, used for $v=6$ and 7 bands. The precision of the measurement is estimated as 0.02 cm^{-1}. The absorption linewidth is about 0.05 cm^{-1} (HWHM).

Another highly sensitive laser technique suitable for overtone spectroscopic study is laser photoacoustic spectroscopy (LPAS). The advantages of this method are the high sensitivity and continuous tunability of Dye/Ti–sapphire lasers. One of the most sensitive LPAS techniques is intracavity dye laser photoacoustic spectroscopy (ICL-PAS), which was first applied to gas phase overtone spectroscopy by Stella, Gelfand and Smith [20], and then used to study a series of overtone spectroscopes of XH_n type molecules by Reddy and Berry [21,22], Henry and co-workers [23]. Halonen and co-workers have used intracavity Dye/Ti–sapphire laser photoacoustic technique to obtain the high resolution spectra of SnH_4 stretching overtones [5–8]. However, owing to the limited available space inside a laser cavity, ICL-PAS is a very sophisticated and difficult technique.

Since photoacoustic signal intensity is sensitively dependent on the chopping frequency, the photoacoustic sensitivity may greatly increase if we use a sharp resonant chopping frequency. However, since the photoacoustic cell used in ICL-PAS is small and its geometry can not be best designed, this resonant chopping frequency is usually so high that it is difficult to be found in practice. In the present study, we have made a novel multipath photoacoustic cell and recorded the high resolution photoacoustic spectrum of arsine $v=6$ stretching overtones (600) in the region 11 470–11 650 cm^{-1}. The upper state was found strongly perturbed. The vibration–rotation transitions were partially assigned and discussed.

2. Experimental method and results

The high resolution spectrum in the region of 11 470–11 650 cm^{-1} was recorded by a sensitive laser photoacoustic apparatus specially made in our laboratory. A titanium–sapphire ring laser (Coherent 899-29) was used to excite the arsine molecules. The induced photoacoustic signal was detected by a microphone (with sensitivity of 5 mV Pa^{-1}), placed in the middle (on the wall) of a stainless steel cylinder with 100 cm in length and 12 cm in diameter. The laser beam was reflected and re-focused many times by two sets of mirrors at both ends of the gas cell (for more details see Ref. [24]). Fixing the chopping frequency at 2008 Hz, which is the acoustic resonant frequency of the first radial mode with arsine gas inside, and using the effective path length of 72 m, we recorded the spectrum with the sample pressure of 30 Torr at room temperature (293 K). AsH_3 was purchased from Nanjing Special Gas Company with the purity of 99.99%. In the experiment, the laser power was 1.0 W and its wavelength was calibrated by the lines of H_2O [25], which was mixed with AsH_3 in the cell in a separate experiment. The resolution was limited by Doppler linewidth (about 0.023 cm^{-1}), and the accuracy of measurement was about 7×10^{-3} cm^{-1}. Fig. 1 shows a survey of the spectrum recorded.

The intensities of the vibration–rotational transitions of ($600A_1/E$) bands were estimated. Fig. 2(a) is the spectrum of 30 Torr pure AsH_3, and Fig. 2(b) is that of 28 Torr AsH_3 with 4.5 Torr water vapor in the cell. Two water lines appear clearly in Fig. 2(b). From the intensity (1.08×10^{-26} cm mol^{-1}) of one unblended water line at 11 588.515 cm^{-1} [25], the intensity of the nearby AsH_3 line at 11 589.610 cm^{-1} (marked by an asterisk in Fig. 2) was estimated to be 5.1×10^{-27} cm mol^{-1}. In turn, the intensity of the strongest AsH_3 lines at 11 573.809 cm^{-1} in the ($600A_1/E$) band was estimated to be 1.4×10^{-26} cm mol^{-1}. In the same way, the observed strongest lines around 11 960 cm^{-1}, which may be assigned to be that of AsH_3 (510) bands, were estimated with the intensity of about 5×10^{-28} cm mol^{-1}.

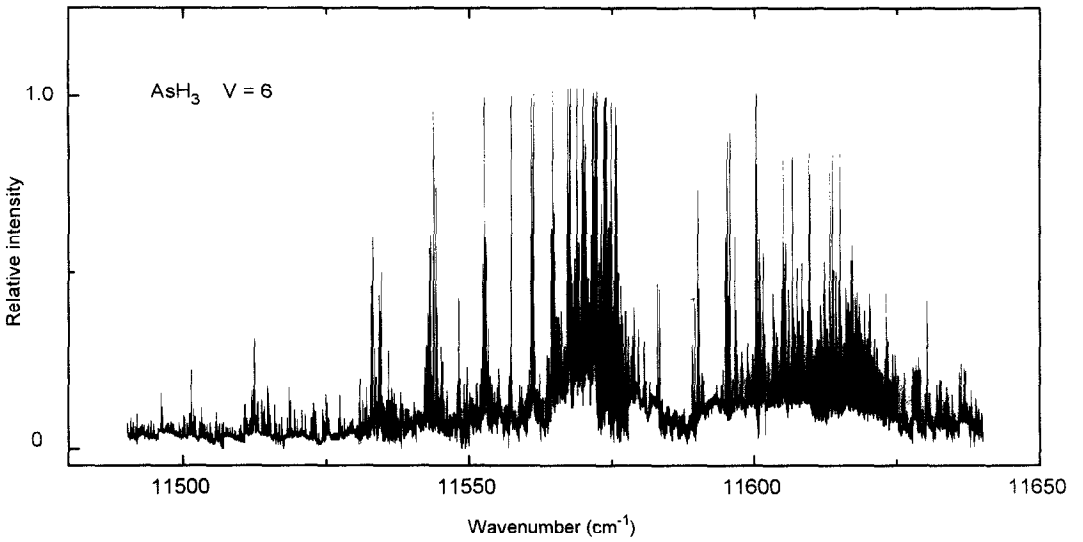

Fig. 1. The high resolution photoacoustic spectrum of arsine ($600A_1/E$) bands.

3. Rotational assignment

The ground state combination differences method is usually helpful in assigning vibration–rotational spectra. However, it was not so in our case because there were many strong perturbations: only in a few cases could combination differences with three allowed P, Q and R transitions be found, in most cases there were only those with two allowed transitions with some forbidden transitions. Fortunately, AsH_3 is a molecule close to the local mode limit and the vibration–rotational energy structures of its first three stretching local mode overtones have been studied, therefore we can reasonably well predict the vibration–rotational energy levels of unperturbed (600) states by using the results we obtained earlier [12–14].

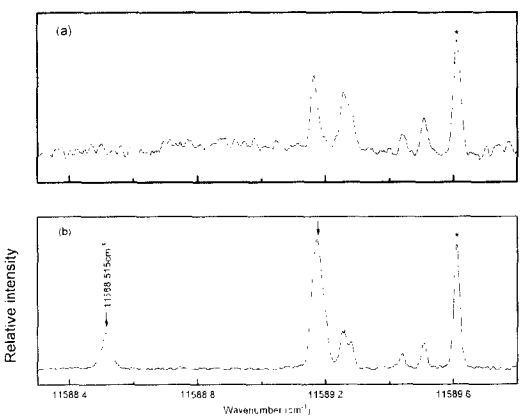

Fig. 2. The spectra in two experiments, (a) with 30 Torr pure AsH_3; (b) with 28 Torr AsH_3 and 4.5 Torr water vapor in the cell. Two water lines are marked out by arrows and the nearby AsH_3 line at 11 589.610 cm^{-1} is marked out by an asterisk.

In order to make the prediction, we calculated the effective vibration–rotational parameters of (600) states by using the vibrational wavefunctions obtained in the normal mode model with Darling–Dennison resonance included (NMDD model). In this model [26], there are $(n+2)(n+1)/2$ basis states for the $v=n$ stretching polyad: $nv_1(A_1)$, $(n-1)v_1+v_3(E)$,..., the Darling–Dennison resonance couples the basis states with the same symmetry. In particular, our attention is drawn to the Hamiltonian submatrices with symmetry A_1 and E, respectively. These two Hamiltonian matrices can be set up for a given stretching polyad by using the expressions of the matrix elements given in Ref. [26], and these are then diagonalized so as to obtain the eigenvalues and eigenvectors. The lowest pair of eigenstates of A_1 and E symmetry are almost degenerate and corre-

spond to the local mode state of this polyad. By the least-square fitting of the known stretching band origins including $v=1$ to $v=4$ [12–14,27], we obtained the three parameters of the NMDD model: the Morse frequency $\omega_m = 2199.26\ cm^{-1}$, anharmonicity constant $x_m = -38.39\ cm^{-1}$ and the inter-bond coupling parameter $\lambda = -3.72\ cm^{-1}$. From these parameters we obtain the following band origins and wavefunctions of ($600A_1$/E) local mode states:

$$\nu_{600A_1} = \nu_{600E} = 11\,582.94\ cm^{-1};$$

$$\begin{aligned}\Phi_{600,A_1} &= 0.0851/\sqrt{2}[|0,6^6\rangle + |0,6^{-6}\rangle)] \\ &+ 0.4821/\sqrt{2}[|1,5^3\rangle + |1,5^{-3}\rangle)] \\ &+ 0.4171/\sqrt{2}[|3,3^{-3}\rangle + |3,3^3\rangle)] \\ &+ 0.270|0,6^0\rangle + 0.608|2,4^0\rangle + 0.372|4,2^0\rangle \\ &+ 0.072|6,0^0\rangle; \end{aligned} \quad (1)$$

$$\begin{aligned}\Phi_{600,E\pm} &= 0.148|0,6^{\pm 4}\rangle + 0.248|2,4^{\pm 4}\rangle \\ &+ 0.482|1,5^{\pm 1}\rangle + 0.511|3,3^{\pm 1}\rangle \\ &+ 0.171|5,1^{\pm 1}\rangle + 0.234|0,6^{\mp 2}\rangle \\ &+ 0.496|2,4^{\mp 2}\rangle + 0.263|4,2^{\mp 2}\rangle \\ &+ 0.152|1,5^{\mp 5}\rangle, \end{aligned} \quad (2)$$

where the local mode state eigenvectors Φ_{600,A_1} and $\Phi_{600E\pm}$ are the linear combinations of several normal mode basis, $|v_1,v_3^{l_3}\rangle$.

The Hamiltonian coefficients available from stretching fundamentals (see column 4 of Table 4 in Ref. [12]), combined with the wavefunctions (1) and (2) can predict the following effective parameters (in cm^{-1}) for the ($600A_1$/E) local mode pair according to the expressions given in Refs. [9–11,28]:

$$B_{600A_1} = B_{600E} = 3.5287,$$

$$C_{600A_1} = C_{600E} = 3.3667,$$

$$(C\zeta)_{600E} = (B\zeta\Omega)_{eff} = 0;$$

$$\alpha_{13}^{BC} = 0.183, \quad \alpha_{13}^{BB} = 0.130, \quad q_t = -0.092,$$

$$r_t = 0.032.$$

In the first step of making rotational assignment, parameters α_{13}^{zx}, α_{13}^{xx}, q_t and r_t were fixed to the above predicted values, and the obtained upper energy levels were least-squares fitted to give rise to the preliminary values of B, C and ζ. Then the new set of parameters were used to predict upper energy levels, which were compared with the observed levels to obtain more assignments. Then, the fitting was carried out again to obtain the improved parameters. Repeating this procedure, we obtained 69 upper energy levels up to $J=6$ (see Table 1), totally 198 lines (including some forbidden transitions) were assigned. Due to the weak intensity and the severe perturbations and the inadequacy, it was difficult to assign the $J>6$ energy levels.

4. Vibration–rotational Hamiltonian

In the least square fitting we used the vibration–rotational Hamiltonian matrix including Coriolis resonance interactions between A_1 and E vibrational states [12]. The diagonal matrix elements are:

$$\begin{aligned}&\langle vl; Jk|H|vl; Jk\rangle \\ &= G_v + B_v[J(J+1) - k^2] + C_v k^2 - 2(C\zeta)_v kl \\ &\quad - D_J^v J^2(J+1)^2 - D_{JK}^v J(J+1)k^2 - D_K^v k^4 \\ &\quad + \eta_{vJ} J(J+1)kl + \eta_{vK} k^3 l + \cdots \end{aligned} \quad (3)$$

where the basis functions $|vlJk\rangle = |vl\rangle|Jk\rangle$, $|Jk\rangle$ are the rotational wave functions, v denotes $|600A_1\rangle$ or $|600E^{\pm}\rangle$ vibrational states respectively, and the corresponding vibrational angular momentum quantum number $l=0, \pm 1$ for the A_1 and E vibrational states, respectively. The off-diagonal matrix elements are [9–14]:

$$\begin{aligned}&\langle 600E^+; Jk+1|(H_{21}+H_{23})/hc|600A_1; Jk\rangle \\ &= -\langle 600A_1; Jk+1|(H_{21}+H_{23})/hc|600E^-; Jk\rangle \\ &= \sqrt{2}\{B\Omega\zeta_{eff}^{\zeta_v} + \zeta_{eff}^{v} J(J+1)\}F(J,k) \end{aligned} \quad (4)$$

$$\begin{aligned}&\langle 600E^+; Jk+2|(H_{22}+H_{24})/hc|600E^-; Jk\rangle \\ &= -\frac{1}{2}\{q_{eff} + q_{eff}^J J(J+1) + q_{eff}^k[k^2 + (k+2)^2]\} \\ &\quad F(J,k)F(J,k+1) \end{aligned} \quad (5)$$

$$\begin{aligned}&\langle 600E^-; Jk+1|(H_{22}+H_{24})/hc|600E^+; Jk\rangle \\ &= 2[r_{eff} + r_{eff}^J J(J+1)](2k+1)F(J,k) \end{aligned} \quad (6)$$

Table 1
The rotational energy levels of AsH_3 ($600A_1/E$) states (cm^{-1})

v[a]	J	K	Γ	Obs.	N[b]	Δ[c]	o.-c.[d]	v	J	K	Γ	Obs.	N	Δ	o.-c.
1	0	0	A_1	11 576.337	1		0.40	1	4	4	E	11 643.928		1	−0.80
3	1	1	A_1	11 583.264	1		0.03	3	4	0	E	11 648.118	2	1	1.96
1	1	0	A_2	11 583.418	2	1	1.84	3	4	1	E	11 646.675	5	5	3.95
3	1	1	A_2	11 583.089	1		−2.22	3	4	2	E	11 646.580	3	8	1.59
1	1	1	E	11 583.089	1		−0.48	3	4	3	E	11 645.066	7	13	−2.16
3	1	0	E	11 583.418	2	9	−0.85	3	4	3	E	11 645.333	5	15	3.55
3	1	1	E	11 583.256	1		−0.15	3	4	4	E	11 643.968	1		1.62
1	2	0	A_1	11 597.645	2	2	−1.68	3	5	1	A_1	11 684.648	2	5	1.20
3	2	1	A_1	11 597.167	1		−2.13	3	5	2	A_1	11 682.491	2	4	1.49
3	2	2	A_2	11 596.665	1		3.09	3	5	5	A_1	11 677.921	3	3	−0.53
	2	1	E	11 597.115	4	9	3.77	1	5	0	A_2	11 684.599	4	4	−1.09
1	2	2	E	11 596.636	1		0.86	1	5	3	A_2	11 680.370	2	5	1.18
3	2	0	E	11 597.545	2	3	−0.87	3	5	1	A_2	11 682.585	6	11	−1.86
3	2	1	E	11 597.642	5	4	−3.61	3	5	2	A_2	11 681.092	3	3	0.68
3	2	2	E	11 596.690	4	3	−1.17	3	5	4	A_2	11 679.483	3	6	0.37
1	3	3	A_1	11 616.877	1		−4.05	3	5	5	A_2	11 677.921	3	3	0.02
3	3	2	A_1	11 617.904	1		−1.53	1	5	1	E	11 684.593	4	12	−0.39
1	3	0	A_2	11 610.205	3	7	−0.24	1	5	4	E	11 679.526	4	9	1.12
3	3	1	A_2	11 618.276	3	2	−1.07	1	5	5	E	11 677.879	3	5	1.15
3	3	2	A_2	11 617.565	1		1.11	3	5	0	E	11 684.624	5	10	1.01
1	3	2	E	11 613.756	4	3	3.95	3	5	2	E	11 682.642	6	6	1.21
3	3	0	E	11 619.147	3	2	1.05	3	5	3	E	11 680.946	2	3	−2.54
3	3	1	E	11 619.220	3	2	1.55	3	5	5	E	11 677.801	3	6	2.91
3	3	2	E	11 618.038	3	9	−0.46	3	6	5	A_1	11 719.973	5	3	0.97
3	3	3	E	11 616.796	3	4	0.37	3	6	5	A_2	11 719.973	3	5	−2.07
1	4	3	A_1	11 645.055	2	5	−4.09	1	6	1	E	11 728.959	3	5	−2.44
3	4	1	A_1	11 646.673	3	3	2.14	1	6	4	E	11 722.549	5	6	−1.14
3	4	2	A_1	11 645.685	2	5	−4.06	1	6	5	E	11 720.819	5	4	0.77
3	4	4	A_1	11 643.885	3	4	0.55	3	6	2	E	11 726.550	4	9	2.15
1	4	3	A_2	11 645.314	1		1.32	3	6	3	E	11 723.991	4	6	−1.70
3	4	1	A_2	11 648.119	2	8	−0.51	3	6	4	E	11 724.361	2	4	2.28
3	4	2	A_2	11 646.484	3	11	−3.30	3	6	5	E	11 721.123	2	2	−2.19
3	4	4	A_2	11 643.885	2	9	−0.29	3	6	6	E	11 718.216	4	8	0.21
1	4	1	E	11 648.091	4	6	−2.38	3	6	6	E	11 718.563	2	4	−1.50
1	4	2	E	11 645.827	4	7	2.12								

Ground state rotational energy levels were taken from Ref. [37].
[a] $v = 1, 3$ denote $|600A_1\rangle$ and $|600E\rangle$ states, respectively.
[b] N is the number of observed lines satisfying the ground state combination difference relation.
[c] $\Delta \times 10^{-3}$ cm^{-1} is the largest energy difference of the upper states obtained from these N lines.
[d] (o.-c.) $\times 10^{-2}$ cm^{-1} is the observed minus calculated value.

$$\langle 600A_1; Jk+2|(H_{22}+H_{24})/hc|600E^+; Jk\rangle = \langle 600E^-; Jk+2|(H_{22}+H_{24})/hc|600A_1; Jk\rangle = \frac{\sqrt{2}}{4}[\alpha_{\text{eff}}^{BB} + \alpha_{\text{eff}}^{BB,J} J(J+1)]F(J,k)F(J,k+1) \quad (7)$$

$$\langle 600E^+; Jk+1|(H_{22}+H_{24})/hc|600A_1; Jk\rangle = \langle 600A_1; Jk+1|(H_{22}+H_{24})/hc|600E^-; Jk\rangle = \frac{\sqrt{2}}{4}[\alpha_{\text{eff}}^{BC} + \alpha_{\text{eff}}^{BC,J} J(J+1)](2k+1)F(J,k) \quad (8)$$

where $F(J,k) = \sqrt{J(J+1) - k(K+1)}$.

A set of parameters, which were obtained from the least squares fitting and reproduced the initial experimental energy levels with the standard deviation $\sigma = 2.25 \times 10^{-2}$ cm^{-1}, is presented in Table 2. It is worth noting that the selection rules on the quantum number k no longer exist, especially for the high J levels owing to the strong Coriolis couplings, and the k structure of the symmetric top parallel band disappears (see Fig. 3). In addition, some unusual lines appear in Fig. 3, maybe due to perturbations.

5. Discussion

Table 3 lists the observed and calculated effective vibration–rotational parameters of arsine stretching local mode pairs. It is interesting to note that some local mode features are clearly demonstrated.

(1) The effective Coriolis coefficients $(B\zeta\Omega)_{\text{eff}}$ and $(C\zeta)_{\text{eff}} \cong 0$; this quenching effect has been predicted by Zhu [29] and others [30–32].

Table 2
The effective rotational parameters for the (600; A_1) and (600; E) stretching states of the AsH_3 molecule (cm^{-1})[a]

Parameters	(600; A_1)	(600; E)
ν	11 576.333(14)	11 576.338(9)
B	3.5284(19)	3.5275(6)
C	3.3228(18)	3.3219(5)
$D_J/10^{-2}$	−0.1039(43)[b]	−0.1039(43)[b]
$\eta_{3K}/10^{-2}$		0.1073
	⟨600; E|600; E⟩	
$r_{\text{eff}}/10^{-1}$		0.3180(106)
$r^J_{\text{eff}}/10^{-2}$		−0.1240(264)
$q_{\text{eff}}/10^{-1}$		−0.7404(65)
$q^J_{\text{eff}}/10^{-2}$		−0.112(23)
$q^k_{\text{eff}}/10^{-2}$		−0.184(27)
	⟨600; A_1|600; E⟩	
α^{BC}_{eff}		0.062(21)
$\alpha^{BCJ}_{\text{eff}}/10^{-2}$		−0.443(52)
α^{BB}_{eff}		0.1057(26)
$\alpha^{BBJ}_{\text{eff}}/10^{-3}$		0.637(84)
$\sigma/10^{-2}$		2.25

[a] Values in parentheses are 1σ confidence intervals.
[b] Parameters D_J for both vibrational states were fixed as equal to each other during the fitting.

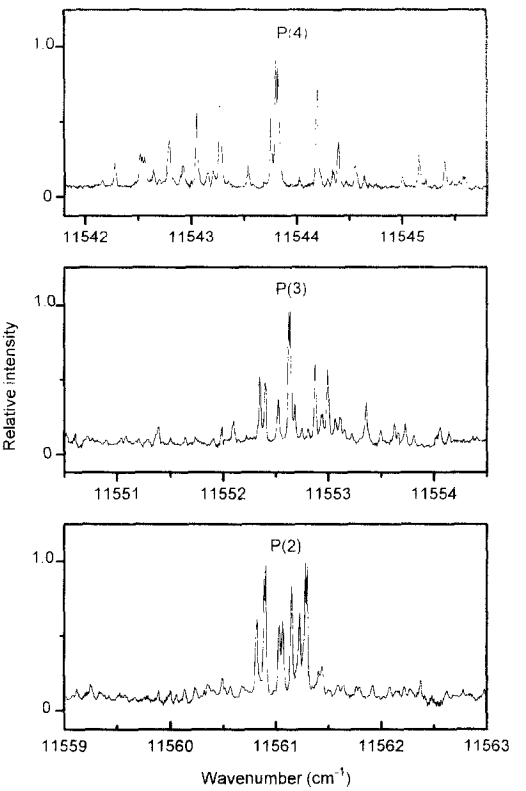

Fig. 3. Expanded picture of the spectra of arsine in the P branch region.

(2) The diagonal parameters of A_1 and E states become equal,

$$\alpha^B_{A_1,\text{eff}} = \alpha^B_{E,\text{eff}}, \qquad \alpha^C_{A_1,\text{eff}} = \alpha^C_{E,\text{eff}}.$$

This is a consequence of the complete mixing of A_1/E pair of states due to the strong vibration–rotation interactions [30–33].

(3) The obtained off-diagonal parameters do not agree well with the predicted simple relationship (see Table 4) for the off-diagonal parameters: $\alpha^{BB}_{\text{eff}} = -\sqrt{2}q_{\text{eff}}$, $\alpha^{BC}_{\text{eff}} = 4\sqrt{2}r_{\text{eff}}$, this may be a consequence of perturbations [28,34,35]. In Table 4, the observed values of the ν_1 band origin have been well predicted by the NMDD model except for the (600) state. This may be the result of perturbations also.

It is known that the bending band origins of the XH_3 molecules are usually below half of the stretching. However, the state involving one local

Table 3
Vibrational dependence of the vibration–rotation parameters (cm^{-1})

	$(100A_1/E)$	$(200A_1/E)$		$(300A_1/E)$		$(400A_1/E)$		$(600A_1/E)$	
	Obs.	Obs.	Calc.	Obs.	Calc.	Obs.	Calc.	Obs.	Calc.
$\alpha^B_{A_1}$	0.03728	0.07597	0.07407	0.11475	0.11138	0.15569	0.14855	0.2232	0.2229
α^B_E	0.03751	0.07550	0.07426	0.11357	0.11139	0.15805	0.14855	0.2241	0.2229
$\alpha^C_{A_1}$	0.0321	0.04805	0.04821	0.05705	0.06704	0.08985	0.08847	0.1758	0.1318
α^C_E	0.0160	0.04358	0.04449	0.06202	0.06684	0.09011	0.08846	0.1766	0.1318
q	−0.005823	−0.030455	−0.02944	−0.04772	−0.04631	−0.06324	−0.06163	−0.0740	−0.0921
r	0.00549	0.01150	0.01074	0.01616[a]	0.01616	0.02157[a]	0.02157	0.03180	0.0324
α^{BB}	0.02827	0.0462	0.0454	0.06836	0.06570	0.08995	0.08717	0.1057	0.1303
α^{BC}	0.03028	0.0628	0.0605	0.09219	0.09140	0.12345	0.12201	0.062	0.183
$B\zeta\Omega$	0.1073	0.0244	0.0240	0.00128	0.00130	0	0.00004	0	0.0000
$C\zeta^z$	−0.0460	−0.01378	−0.00823	−0.00049	−0.00048	0	−0.00001	0	0.0000

Data of the $(100A_1/E)$ states are from Refs. [12,27]; those of the $(200A_1/E)$, $(300A_1/E)$ and $(400A_1/E)$ states are from Refs. [12,13], respectively; and those of the $(600A_1/E)$ state are from this work. The values calculated by the NMDD model.
[a] Constrained to the calculated values.

Table 4
Local mode relations about off-diagonal parameters for the $(100A_1/E)$, $(200A_1/E)$, $(300A_1/E)$, $(400A_1/E)$ and $(600A_1/E)$ local mode pairs

	q_{eff}:α^{BB}_{eff}		r_{eff}:α^{BC}_{eff}		ν_1 (cm^{-1})	
	Obs.	Calc.	Obs.	Calc.	Obs.	Calc.
$100A_1/E$	−0.287:1.414		1:5.908		2115.164	2115.06
$200A_1/E$	−0.932:1.414	−0.918:1.414	1:5.461	1:5.633	4166.772	4166.65
$300A_1/E$	−0.987:1.414	−0.996:1.414	1:5.705	1:5.656	6136.316	6136.58
$400A_1/E$	−0.994:1.414	−0.997:1.414	1:5.723	1:5.657	8028.977	8028.85
$600A_1/E$	−0.991:1.414	−1.00:1.414	1:1.950	1:5.657	11 576.333	11 582.94
LM limit		−1:1.414		1:5.657		

mode pair and double bending excitation modes will hopefully catch up with the next pure local mode states in the high vibrational energy region due to the large stretching anharmonicity. Thus interactions can be expected to occur between these two states. In the range of $(600A_1/E)$ states, perturbations may come from $(500A_1/E) + 2\nu_2$ combination bands. This is because the $2\nu_2$ band origin is 1806.15 cm^{-1} [36] and $500A_1/E$ band origins are equal to 9844.28 cm^{-1} (predicted by NMDD model). Considering the effect of anharmonicity, the $(500A_1/E) + 2\nu_2$ bands should be very close to $(600A_1/E)$ states.

Acknowledgements

This work is supported by the National Natural Science Foundation of China and the Chinese Academy of Science and, in part, by the Russian Foundation on Fundamental Research.

References

[1] Q.-S. Zhu, B.A. Thrush and A.G. Robiette, Chem. Phys. Lett. 150 (1988) 181.
[2] Q.-S. Zhu and B.A. Thrush, J. Chem. Phys. 92 (1990) 2619.
[3] Q.-S. Zhu, B.-S. Zhang, Y.-R. Ma and H.-B. Qian, Spectrochim. Acta 46A (1990) 1217 and 1323.

[4] Q.-S. Zhu, H.-B. Qian, H. Ma and L. Halonen, Chem. Phys. Letts. 177 (1991) 261.
[5] M. Halonen, L. Halonen, H. Bürger and S. Sommer, J. Chem. Phys. 93 (1990) 1607.
[6] M. Halonen, L. Halonen and H. Bürger, Chem. Phys. Lett. 205 (1993) 380.
[7] M. Halonen and X. Zhan, J. Chem. Phys. 101 (1994) 950.
[8] X. Zhan, M. Halonen, L. Halonen, H. Bürger and O. Polanz, J. Chem. Phys. 102 (1995) 3911.
[9] M. Halonen, L. Halonen, H. Bürger and P. Moritz, J. Chem. Phys. 95 (1991) 7099.
[10] M. Halonen, L. Halonen, H. Bürger and P. Moritz, Chem. Phys. Lett. 203 (1993) 157.
[11] J. Lummila, T. Lukka, L. Halonen, H. Bürger and O. Polanz, J. Chem. Phys. 104 (1996) 488.
[12] O.N. Ulenikov, F.-G. Sun, X.-G. Wang and Q.-S. Zhu, J. Chem. Phys. 105 (1996) 7310.
[13] S.-F. Yang, X.-G. Wang and Q.-S. Zhu, Spectrochim. Acta, A53 (1997) 157.
[14] J.-X. Cheng, X.-G. Wang, H. Lin and Q.-S. Zhu, Chin. Phys. Lett., accepted.
[15] O.N. Ulenikov, A.B. Malikova, H.F. Li, H.B. Qian, Q.S. Zhu and B.A. Thrush, J. Chem. Soc., Faraday Trans. 91 (1) (1994) 13.
[16] O.N. Ulenikov, A.B. Malikova, H.F. Li, H.B. Qian, Q.S. Zhu and B.A. Thrush, Spectrochim. Acta A 50 (1994) 2731.
[17] A. Campargue, F. Stoeckel and M. Chenevier, Spectrochim. Acta Rev. 13 (1990) 69.
[18] Q.S. Zhu, A. Campargue and F. Stoeckel, Spectrochim. Acta 50A (1994) 663.
[19] Q.S. Zhu, A. Campargue, J. Vetterhöffer, D. Permogorov and F. Stoeckel, J. Chem. Phys. 99 (1993) 2359.
[20] G. Stella, J. Gelfand and W.H. Smith, Chem. Phys. Lett. 39 (1976) 146.
[21] K.V. Reddy and M.J. Berry, Chem. Phys. Lett. 52 (1977) 111.
[22] K.V. Reddy and M.J. Berry, Faraday Disc. Chem. Soc 67 (1979) 146.
[23] B.R. Henry, H.G. Kjaergaard, B. Niefer, B.J. Schattka and D.M. Turnbull, Can. J. Appl. Spectr. 38 (1993) 42.
[24] L.-Y. Hao, J.-X. Han, J.-H. Zhang and Q.-S. Zhu, in preparation.
[25] N. Husson, A. Chedin, N.A. Scott et al., Ann. Geophys. 4A (1986) 185.
[26] I.M. Mills and A.G. Robiette, Mol. Phys. 56 (4) (1985) 743.
[27] O.L. Ulenikov, A.E. Cheglokov, G.A. Shevchenko, M. Winnewiser and B. Winnewiser, J. Mol. Spectrosc. 157 (1993) 141.
[28] X.-G. Wang and Q.-S. Zhu, J. Chem. Phys. 105 (1996) 8011.
[29] Q.-S. Zhu, H.-F. Li and X.-G. Wang, Chem. Phys. Lett. 212 (1993) 403.
[30] L. Halonen and A.G. Robiette, J. Chem. Phys. 84 (1986) 6861.
[31] L. Halonen, J. Chem. Phys. 86 (1987) 588.
[32] K. Lehman, J. Chem. Phys. 95 (1991) 2361.
[33] Q. Zhu, Spectrochim. Acta 48A (1992) 193.
[34] T. Lukka and L. Halonen, J. Chem. Phys. 101 (1994) 8380.
[35] T. Lukka, E. Kauppi and L. Halonen, J. Chem. Phys. 102 (1995) 5200.
[36] O.L. Ulenikov, A.B. Malikova, B.P. Winnewisser and M. Winnewisser, J. Mol. Spectrosc. 172 (1995) 330.
[37] M. Carlotti, G. Dilonardo and L. Fusina, J. Mol. Spoectrosc. 102 (1983) 310.